

CEBAF Program Advisory Committee Eight Cover Sheet

This proposal must be received by close of business on Thursday, April 14, 1994 at:

CEBAF

User Liaison Office, Mail Stop 12 B

12000 Jefferson Avenue

Newport News, VA 23606

Proposal Title

Measurements of Transverse Polarization Observables in
the $d(\vec{e}, e'\vec{n})p$ Reaction

Contact Person

Name: Bryon D. Anderson

Institution: Kent State University

Address: Physics Department

Address: Kent State University

City, State ZIP/Country: Kent, OH 44242

Phone: (216) 672-2771 **FAX:** (216) 672-2959

E-Mail → Internet: Anderson@KSUVXD.Kent.Edu

Experimental Hall: Hall C

Total Days Requested for Approval: 20

Minimum and Maximum Beam Energies (GeV): 1.6

Minimum and Maximum Beam Currents (μ Amps): 0.67-5.0

CEBAF Use Only

Receipt Date: 4/14/94 1294-007

By: [Signature]

HAZARD IDENTIFICATION CHECKLIST

Transverse Polarization Observables in $d(e^+, e^+ n^0)$ Reacti

CEBAF Experiment: PR-94-007

Date: 5/31/94

Check all items for which there is an anticipated need—do not check items that are part of the CEBAF standard experiment (HRSE, HRSH, CLAS, HMS, SOS in standard configurations).

B.D. Anderson et al.

Cryogenics <input type="checkbox"/> beamline magnets <input type="checkbox"/> analysis magnets <input checked="" type="checkbox"/> target <input type="checkbox"/> drift chambers <input type="checkbox"/> other	Electrical Equipment <input type="checkbox"/> cryo/electrical devices <input type="checkbox"/> capacitor banks <input type="checkbox"/> high voltage <input type="checkbox"/> exposed equipment	Radioactive/Hazardous Materials List any radioactive or hazardous/toxic materials planned for use: <u>Liquid hydrogen (deuterium) target</u>
Pressure Vessels <input type="checkbox"/> inside diameter <input type="checkbox"/> operating pressure <input type="checkbox"/> window material <input type="checkbox"/> window thickness	Flammable Gas or Liquids (incl. target) type: <u>LHz, LDz</u> flow rate: _____ capacity: _____ <u>15 cm long,</u> <u>"standard" Hall C</u> <u>target.</u>	Other Target Materials <input type="checkbox"/> Beryllium (Be) <input type="checkbox"/> Lithium (Li) <input type="checkbox"/> Mercury (Hg) <input type="checkbox"/> Lead (Pb) <input type="checkbox"/> Tungsten (W) <input type="checkbox"/> Uranium (U) <input type="checkbox"/> Other (list below) _____ _____
Vacuum Vessels <input type="checkbox"/> inside diameter <input type="checkbox"/> operating pressure <input type="checkbox"/> window material <input type="checkbox"/> window thickness	Radioactive Sources <input type="checkbox"/> permanent installation <input checked="" type="checkbox"/> temporary use type: <u>228 Th</u> strength: <u>10 μC</u> <u>(For calibrating neutron detectors.)</u>	Large Mech. Structure/System <input type="checkbox"/> lifting devices <input type="checkbox"/> motion controllers <input type="checkbox"/> scaffolding or elevated platforms <input checked="" type="checkbox"/> other
Lasers type: _____ wattage: _____ class: _____ Installation <input type="checkbox"/> permanent <input type="checkbox"/> temporary Use <input type="checkbox"/> calibration <input type="checkbox"/> alignment	Hazardous Materials <input type="checkbox"/> cyanide plating materials <input type="checkbox"/> scintillation oil (from) <input type="checkbox"/> PCBs <input type="checkbox"/> methane <input type="checkbox"/> TMAE <input type="checkbox"/> TEA <input type="checkbox"/> photographic developers <input type="checkbox"/> other (list below) _____ _____ _____	Notes: <u>Need large concrete</u> <u>steel shielding</u> <u>enclosure for neutron</u> <u>detectors (same</u> <u>as for approved</u> <u>Ge^+ exp.).</u>

**Measurements of Transverse Polarization Observables
in the $d(\vec{e}, e'\vec{n})p$ Reaction**

SCIENTIFIC PARTICIPANTS

Kent State University

Kent, OH 44242

B. Anderson (Spokesman)

R. Madey (Spokesman)

W. Zhang (Spokesman)

A. Baldwin

A. Lai

M. Manley

G. Petratos

J. Watson

Graduate Student(s)

Hampton University

Hampton, VA 23688

R. Madey (Spokesman)

K. Baker

K. Beard

S. Beedoe

T. Eden

L. Tang

Graduate Student(s)

CEBAF

Newport News, VA 23606

C. Yan

University of Mainz

Mainz, Germany

H. Arenhövel

College of William and Mary

Williamsburg, VA 23185

M. Finn

University of Virginia

Charlottesville, VA 22901

R. Lourie

Gettysburg College

Gettysburg, PA 17325

P. Pella

Old Dominion University

Norfolk, VA 23508

P. Ulmer

University of Maryland

College Park, MD 20742

P. Markowitz

CONTENTS

Abstract	1
1. Introduction and Physics Motivation	2
2. Theoretical Background	4
2.1 Formalism	4
2.2 Predictions	7
3. Experimental Arrangement	9
3.1 Electron Spectrometer	11
3.2 Neutron Polarimeter	11
3.3 Steel Collimator and Shielding	14
4. Design of the Experiment	15
4.1 Kinematics	15
4.2 Conditions of Neutron Polarimeter and HMS	16
4.3 Beam and Targets	16
4.4 Counting Rates and Backgrounds	16
4.4.1 Counting Rates	17
4.4.2 Accidental Backgrounds	17
4.4.3 Backgrounds from Inelastic Processes	17
4.5 Statistics and Uncertainties	18
5. Beam Time Request	18
References	20
Appendix A: Experimental Conditions	22
Appendix B: Counting Rate and Background at Kinematics K^0	24

Abstract

We propose to measure the two polarization response functions $R_{TT'}^t$ and $R_{LT'}^t$ in the $d(\vec{e}, e'\vec{n})p$ reaction at $Q^2 = 0.30 \text{ (GeV/c)}^2$ with a polarized electron beam of 1.6 GeV. The measurements will be performed at $\theta_{nq}^{cm} = 38^\circ$ by detecting neutrons on each side of \vec{q} in quasi-perpendicular kinematics; θ_{nq}^{cm} is the angle of the emitted neutron with respect to the three momentum transfer in the center-of-mass system of the deuteron. These measurements are expected to be sensitive to final-state interactions, meson-exchange currents, and relativistic effects, and are intended to provide tests of various models of these effects. These measurements will complement similar measurements of the proton polarization in the electrodisintegration of the deuteron. Measurements of response functions from a recoil neutron in the $d(\vec{e}, e'\vec{n})p$ reaction are essential for a complete description of deuteron electrodisintegration. This experiment will begin to provide the necessary neutron measurements and will allow one to look for differences between the neutron and proton measurements.

1 Introduction and Physics Motivation

The electrodisintegration of the deuteron is a relatively simple process and allows one to study both nuclear and subnuclear degrees of freedom [Si79, Au85]. At low energies, the process is especially useful for the study of the deuteron wave function and the NN interaction [Ar91]. At higher energies, the process becomes sensitive to meson-exchange currents (MEC), isobar configurations (IC), relativistic corrections (RC), and, eventually, to quark-gluon degrees of freedom.

We propose to measure the transverse polarization of the ejected neutron in the $d(\vec{e}, e'\vec{n})p$ reaction using a longitudinally polarized electron beam. Separate proposals have been approved at Bates [UI91] and at CEBAF [Fi89] to measure the polarization of the proton in the complementary $d(\vec{e}, e'\vec{p})n$ reaction. Picklesimer and Van Orden [Pi87, Pi89] have shown that 18 independent amplitudes are required to describe deuteron electrodisintegration. Dmitrasinovic and Gross [Dm89] have shown that in the general case, when the incoming electron, deuteron target, and the outgoing nucleon may all be polarized, deuteron electrodisintegration leads to 162 observables. Most of these observables can be measured by detecting either the emitted proton or neutron; however, Dmitrasinovic and Gross have shown that *at least one* measurement of a recoil neutron polarization is required for a complete program of measurements, and have indicated that ideally there should be a *balanced* set of both neutron and proton measurements. This proposal is designed to provide the first neutron measurements at non-quasifree kinematics.

The kinematics for the $d(\vec{e}, e'\vec{n})p$ reaction are illustrated in Fig. 1. We use the term *quasifree* kinematics to refer to the kinematic condition that the momentum of the ejected nucleon is along \vec{q} and $\vec{P}'_r = 0$, where \vec{P}'_r is the recoil momentum of the other nucleon. If the energy transfer satisfies $\omega = Q^2/(2m)$, so that the struck nucleon is not excited, then we refer to the reaction as having *quasielastic* kinematics; in general, $\vec{P}'_r \neq 0$ for *quasielastic* kinematics. Finally, if \vec{P}'_r is approxi-

mately perpendicular to \vec{P}_r , we refer to the reaction as having *quasi-perpendicular* kinematics. It can be shown that this condition is obtained if $|\vec{P}'| = |\vec{q}|$ [Fr84].

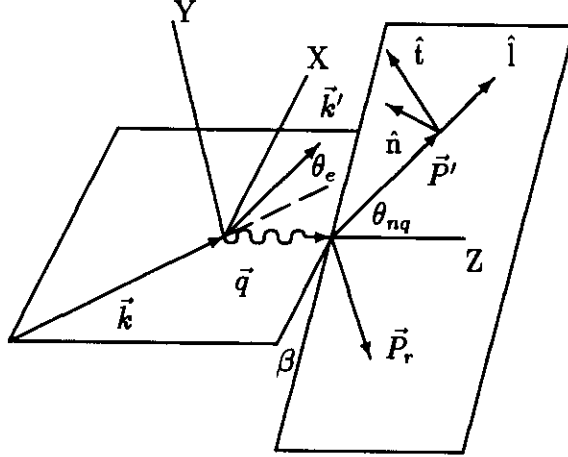


FIG. 1: Kinematic diagram of $d(\vec{e}, e'\vec{n})p$.

At quasifree kinematics, the Impulse Approximation (IA) has been shown to provide a reasonable description of the nucleon knock-out process. In this approximation, the cross section factors into a nuclear spectral function containing all the nuclear structure information, and a part that describes the interaction of the electron with a constituent nucleon [Mo76]. As one moves away from quasifree kinematics, *i.e.*, away from $P_r = 0$, model dependencies can become important, including final-state interactions (FSI) and MEC. As mentioned earlier, we are interested in measuring spin observables from the $d(\vec{e}, e'\vec{n})p$ reaction. In quasifree (QF) kinematics in the IA, the sideways polarization component yields the ratio G_E^n/G_M^n , where G_E^n and G_M^n are the electric and magnetic form factors of the neutron, respectively [Ar81]. The first experiment to measure G_E^n from the $d(\vec{e}, e'\vec{n})p$ reaction was successful at Bates [Ed94], and another is approved at CEBAF (E93-

038). Analyses by Arenhövel [Ar94] show that the G_E^n experiment should be relatively insensitive to the details of the nuclear model, FSI, and MEC.

This proposal is to perform a similar measurement, with the same experimental equipment used for measuring G_E^n [Ma94], but to move away from QF kinematics, so that $P_r \neq 0$, where calculations indicate sensitivity to the inelastic effects, including FSI and MEC. For example, in the IA, for QF parallel kinematics the normal component of the neutron polarization vanishes; however, away from QF parallel kinematics, Arenhövel has shown that this polarization can become quite large when FSI and MEC are included [Ar94, Pi89]. Relativistic effects may also be significant [Hu94, Wi93]. Ultimately, one will test how well such measurements can be described satisfactorily in terms of these effects, *i.e.*, FSI, relativistic effects, *etc.*. The neutron measurements proposed here are to provide a *first look* at the neutron polarizations, and will be compared to the planned proton measurements. Although some of the effects to be studied may be expected to be approximately the same for either neutron or proton observables, some of these effects may be quite different. For example, since the neutron interaction (magnetic) is much weaker than the proton interaction (electric), it is likely that the proton plus MEC diagram will feed into the neutron channel faster than the neutron plus MEC diagram will feed into the proton channel; hence, the effects of MEC may be rather different. In general, it is important to spend at least a modest amount of time to look at the neutron response functions in order to compare with the proton response functions.

2 Theoretical Background

2.1 Formalism

The differential cross section for the $d(\vec{e}, e'\vec{n})p$ reaction can be written as [Pi89]

$$\frac{d^3\sigma}{d\omega d\Omega_e d\Omega_n} = \frac{1}{2}\sigma_M\{V_L(R_L + R_L^n S_n) + V_T(R_T + R_T^n S_n)\}$$

$$\begin{aligned}
& +V_{TT}[(R_{TT} + R_{TT}^n S_n) \cos 2\beta + (R_{TT}^l S_l + R_{TT}^t S_t) \sin 2\beta] \\
& +V_{LT}[(R_{LT} + R_{LT}^n S_n) \cos \beta + (R_{LT}^l S_l + R_{LT}^t S_t) \sin \beta] \\
& +hV_{LT'}[(R_{LT'} + R_{LT'}^n S_n) \sin \beta + (R_{LT'}^l S_l + R_{LT'}^t S_t) \cos \beta] \\
& +hV_{TT'}(R_{TT'}^l S_l + R_{TT'}^t S_t)\}, \tag{1}
\end{aligned}$$

where ω is the energy transfer, the R 's are response functions, the V 's are known kinematic factors, the S 's are the three components of \hat{S}_n , β is the azimuthal angle between the electron scattering plane and the plane containing \vec{q} and the ejectile neutron, and h is the helicity of the incident electron. Here,

$$\sigma_M = \frac{m|\mathbf{P}'|}{(2\pi)^3} \left[\frac{d\sigma}{d\Omega_e} \right]_{Mott}. \tag{2}$$

The coordinate system used in describing the $d(\vec{e}, e'\vec{n})p$ reaction is shown in Fig 1.

In terms of the neutron polarization, the coincidence differential cross section can also be expressed as

$$\frac{d^3\sigma}{d\omega d\Omega_e d\Omega_n} = \frac{1}{2}\sigma_0(1 + \vec{p} \cdot \hat{S}_n), \tag{3}$$

where σ_0 is the unpolarized (neutron) cross section and $\vec{p} = p_n\hat{n} + p_l\hat{l} + p_t\hat{t}$ is the ejectile neutron polarization. For coplanar kinematics ($\beta = 0$ or $\beta = \pi$), Eq. (1) simplifies to

$$\begin{aligned}
\frac{d^3\sigma}{d\omega d\Omega_e d\Omega_n} = & \frac{1}{2}\sigma_M\{V_L(R_L + R_L^n S_n) + V_T(R_T + R_T^n S_n) \\
& +V_{TT}(R_{TT} + R_{TT}^n S_n) + V_{LT}(R_{LT} + R_{LT}^n S_n) \cos \beta \\
& +hV_{LT'}(R_{LT'}^l S_l + R_{LT'}^t S_t) \cos \beta + hV_{TT'}(R_{TT'}^l S_l + R_{TT'}^t S_t)\}. \tag{4}
\end{aligned}$$

The unpolarized and the normal, longitudinal, and transverse polarization dependent parts of the differential cross section are, respectively,

$$\sigma_0 = \sigma_M(V_L R_L + V_T R_T + V_{TT} R_{TT} + V_{LT} R_{LT} \cos \beta), \tag{5}$$

$$\sigma_0 p_n = \sigma_M(V_L R_L^n + V_T R_T^n + V_{TT} R_{TT}^n + V_{LT} R_{LT}^n \cos \beta), \tag{6}$$

$$\sigma_0 p_l = \sigma_M h (V_{LT'} R_{LT'}^l \cos \beta + V_{TT'} R_{TT'}^l), \quad (7)$$

$$\sigma_0 p_t = \sigma_M h (V_{LT'} R_{LT'}^t \cos \beta + V_{TT'} R_{TT'}^t). \quad (8)$$

Note that p_n is helicity independent, whereas p_l and p_t are linear in h . In these measurements, we are interested only in the transverse polarization observables that can be measured with a neutron polarimeter. We define the two transverse polarization asymmetries as

$$A_t^\pm = \frac{(\sigma_0 p_t)_{\beta=0} \pm (\sigma_0 p_t)_{\beta=\pi}}{h[(\sigma_0)_{\beta=0} + (\sigma_0)_{\beta=\pi}]}. \quad (9)$$

A_t^+ and A_t^- are proportional to the response functions $R_{TT'}^t$ and $R_{LT'}^t$, respectively. Dmitrasinovic and Gross [Dm89] have shown that at least one measurement of a recoil neutron polarization is required for a complete determination of the 18 deuteron electrodisintegration amplitudes. They point out that the measured neutron polarization observable must be chosen from among eight particular response functions if an unpolarized deuteron target is used. One of the response functions ($R_{LT'}^t$) that we propose to measure is one of these eight special response functions. Picklesimer and Van Orden [Pi89] considered the response functions in a plane-wave impulse approximation; in this approximation they predict that some of the response functions are zero. The two response functions considered here are both predicted to be nonzero and, in fact, $R_{LT'}^t$ is predicted to be large.

The three polarization observables p_t and A_t^\pm can be measured by detecting neutrons from a secondary scattering with a neutron polarimeter. The quantities σ_0 and $\sigma_0 p_t$ can be expressed as functions of N_+^T , N_+^B , N_-^T , and N_-^B , the numbers of neutrons detected in the top and bottom rear detectors of the neutron polarimeter for the positive and negative helicity states of the incident electron; *i.e.*,

$$\sigma_0 = F(N_+^T + N_+^B + N_-^B + N_-^T), \quad (10)$$

$$\sigma_0 p_t = \frac{F}{A_y} (N_+^T - N_+^B + N_-^B - N_-^T), \quad (11)$$

where F is a measurable common proportionality factor depending on the luminosity and detection efficiency, and A_y is the analyzing power of the neutron polarimeter. From Eqs.(9), (10), and (11), we can express the polarization observables and structure functions of interest in terms of the numbers of detected neutrons:

$$p_t = \frac{(N_+^T - N_+^B + N_-^B - N_-^T)}{A_y(N_+^T + N_+^B + N_-^B + N_-^T)}, \quad (12)$$

$$A_t^\pm = \frac{(N_+^T - N_+^B + N_-^B - N_-^T)_{\beta=0} \pm (N_+^T - N_+^B + N_-^B - N_-^T)_{\beta=\pi}}{hA_y[(N_+^T + N_+^B + N_-^B + N_-^T)_{\beta=0} + (N_+^T + N_+^B + N_-^B + N_-^T)_{\beta=\pi}]}, \quad (13)$$

$$R_{TT'}^t = \frac{F[(N_+^T + N_+^B + N_-^B + N_-^T)_{\beta=0} + (N_+^T + N_+^B + N_-^B + N_-^T)_{\beta=\pi}]}{2h\sigma_M V_{TT'}} A_t^+, \quad (14)$$

$$R_{LT'}^t = \frac{F[(N_+^T + N_+^B + N_-^B + N_-^T)_{\beta=0} + (N_+^T + N_+^B + N_-^B + N_-^T)_{\beta=\pi}]}{2h\sigma_M V_{LT'}} A_t^-. \quad (15)$$

2.2 Predictions

As one example of the kind of theoretical calculations that can be performed to compare with the proposed measurements, we present here calculations performed by Arenhövel for the kinematic conditions proposed. Arenhövel calculated p_t and A_t^\pm for the reaction $d(\vec{e}, e'\vec{n})p$ at $Q^2 = 0.30$ (GeV/c)² with a beam energy of 1.6 GeV and a 100% beam polarization. Figure 2 shows the calculated neutron transverse polarization p_t (top panel) and transverse polarization asymmetries A_t^\pm (bottom panel) plotted as a function of θ_{nq}^{cm} ; model dependencies are expected away from $\theta_{nq}^{cm} = 0^\circ$. The angle θ_{nq}^{cm} is equal to $180^\circ - \theta_{np}^{cm}$ in the center-of-mass system; θ_{np}^{cm} is frequently used in the literature about $d(\vec{e}, e'\vec{p})n$ reaction [Fa78, Fi89]. In Fig. 2, the dashed curves are for the PWBA, the solid curves include FSI, and the dotted curves include FSI+MEC+IC. Figure 2 shows that the difference between FSI and PWBA for p_t and A_t^+ becomes significant beyond about $\theta_{nq}^{cm} = 30^\circ$. We propose here to begin with one set of measurements at $\theta_{nq}^{cm} = 38^\circ$; results at $\theta_{nq}^{cm} = 0^\circ$ will be obtained from CEBAF experiment E93-038 to measure G_E^n [Ma94]. (The

angle θ_{nq}^{cm} is limited by how close the neutron polarimeter with its shielding can be placed near the beam line.)

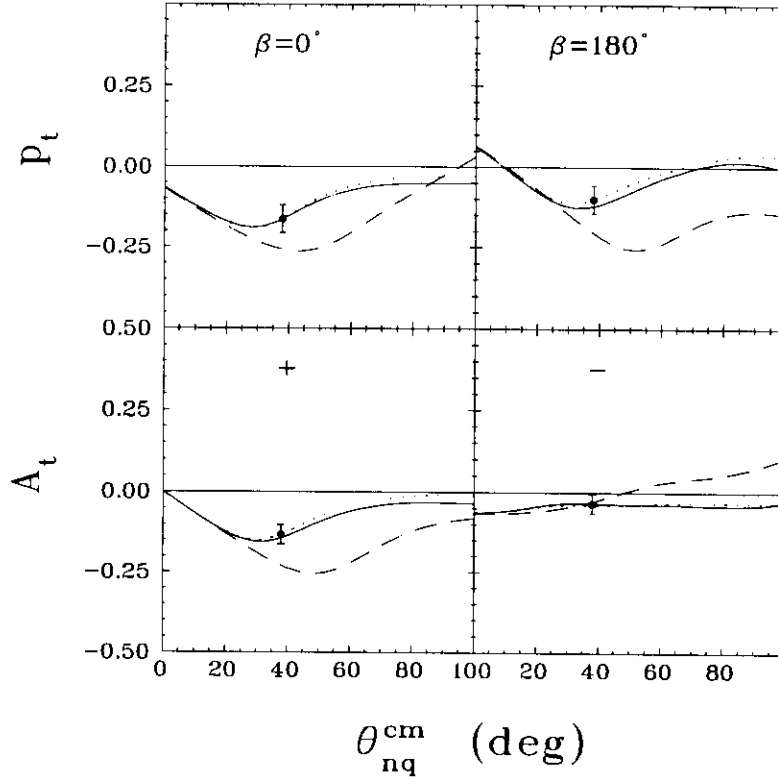


FIG. 2: Neutron Polarization p_t and Asymmetries A_t^\pm for $d(\vec{e}, e'\vec{n})p$ at $E = 1.6$ GeV and $Q^2 = 0.30$ $(\text{GeV}/c)^2$. The dashed curves are for the PWBA, the dotted curves include FSI, and the solid curves include FSI + MEC + IC.

Even without various model dependences, one does not expect neutron and proton measurements to be the same. Shown in Fig. 3 are the predictions of Arenhövel for neutrons compared to protons for p_t and A_t^\pm . One sees that significant differences are expected, even in the PWBA. Of course if the measured differences are due only to the different nucleon form factors, then it is not as important to study both neutrons and protons; however, it is important to perform at least one set of neutron measurements to see if the differences may be explained simply or not. As discussed already, one might expect differences from the different strengths of the electron–neutron and electron–proton interactions and their effects on MEC.

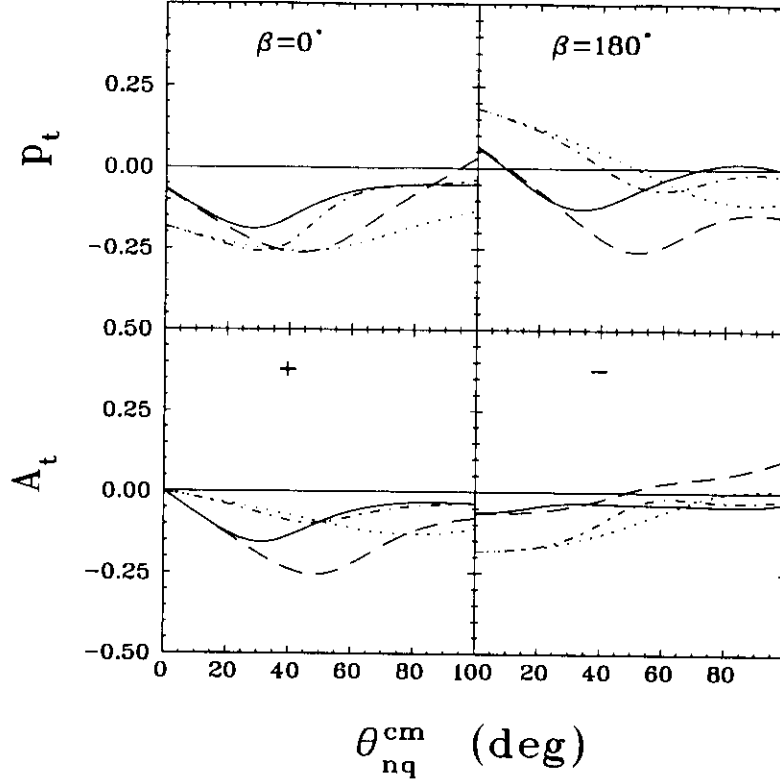


FIG. 3: Nucleon Polarization p_t and Asymmetries A_t^\pm for $d(\bar{e}, e'\bar{n})p$ at $E = 1.6$ GeV and $Q^2 = 0.30$ $(\text{GeV}/c)^2$. The dashed (dotted) curves are for the PWBA for neutron (proton) and the solid (dot-dashed) curves include FSI + MEC + IC for neutron (proton)

3 Experimental Arrangement

The schematic view of the experimental arrangement is shown in Fig. 4. The longitudinally polarized beam will pass through a 15-cm long liquid-deuterium target. The scattered electrons and the ejected neutrons will be detected in coincidence. The electrons will be detected on one side of the beam using the Hall C High Momentum Spectrometer (HMS). The neutrons will be detected on the other side of the beam using a neutron polarimeter. As discussed in Sec. 2, the measurement for a specific θ_{nq}^{cm} requires two angle settings of the neutron polarimeter ($\beta = 0, \pi$) to extract the response functions.

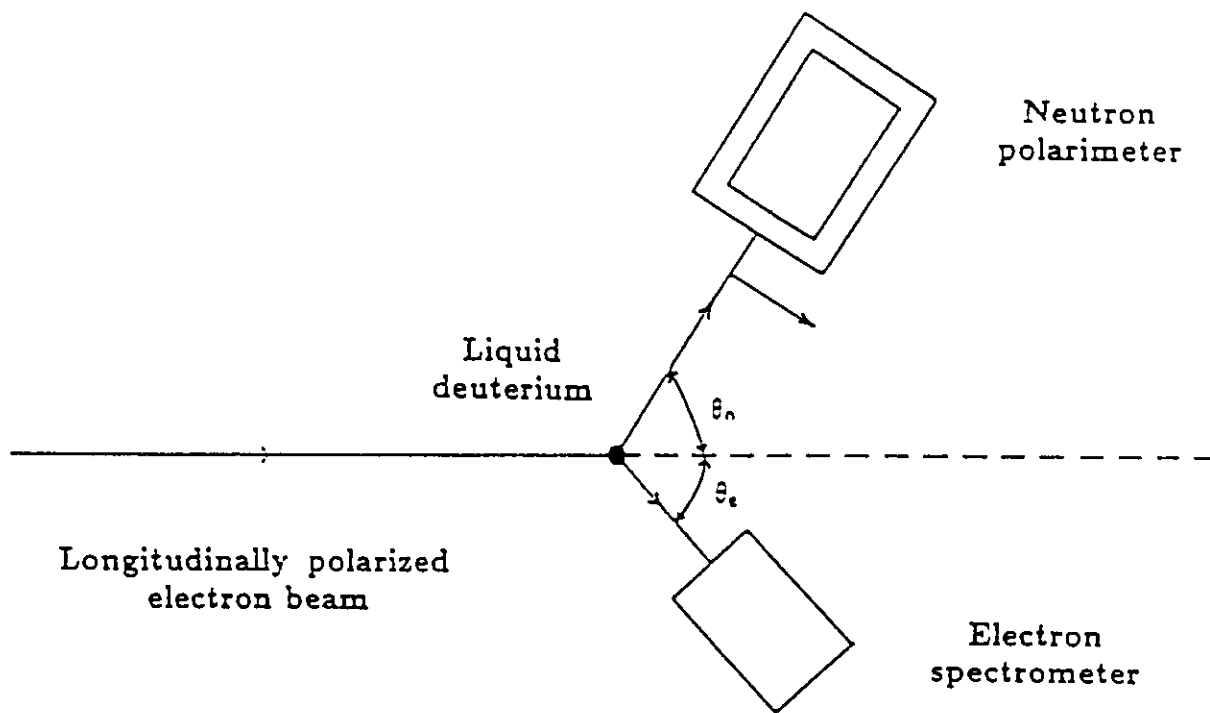


FIG. 4: A schematic view of the experimental arrangement.

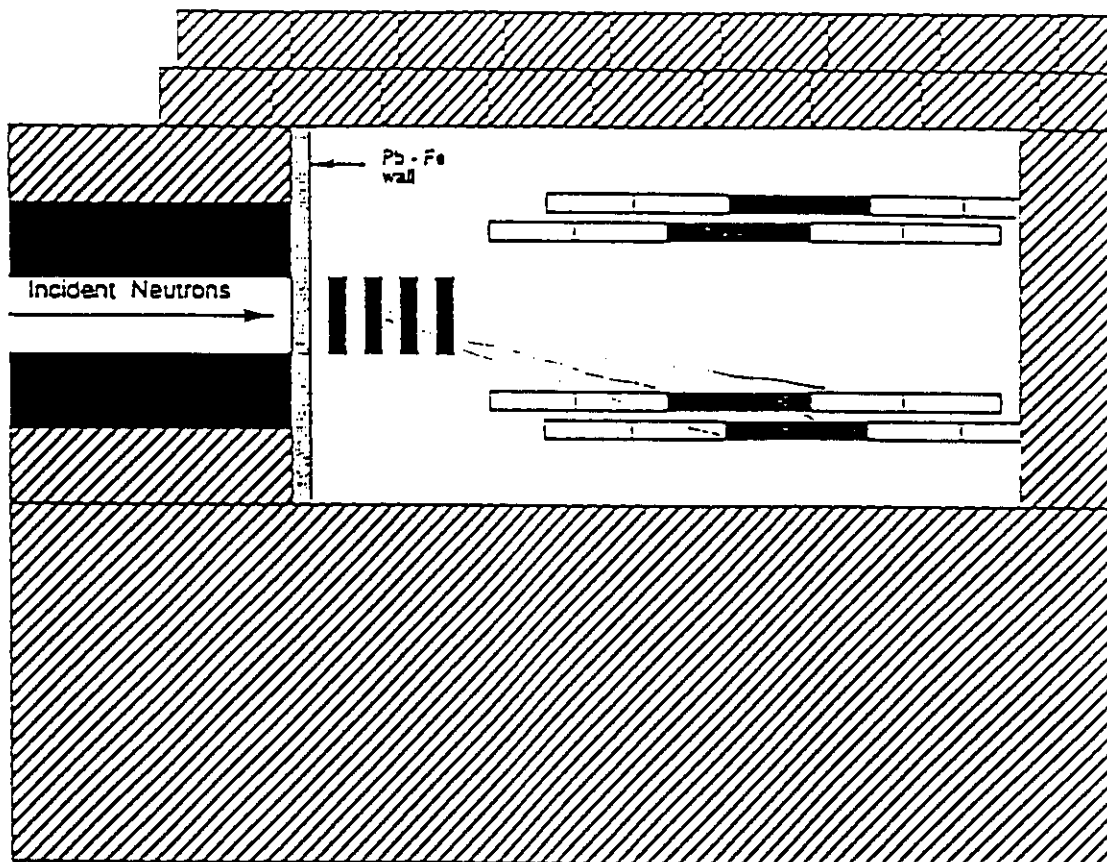
3.1 The Electron Spectrometer

The HMS in HALL C at CEBAF will be used to detect the electrons. The minimum angle between the beam and the magnet is 12.5° . The HMS will be run in the reverse-quad mode; this increases the horizontal acceptance significantly and will more closely match the acceptance of the neutron polarimeter. In this mode, the momentum acceptance is 5% and the momentum resolution $\delta p/p$ is about 0.1%. The horizontal and vertical angular acceptances are ± 62 and ± 22.5 mr, respectively.

3.2 The Neutron Polarimeter

A high-efficiency neutron polarimeter, which was designed to measure G_E^n [Ma94], will be used to detect the neutrons. Basically, it consists of eight plastic scintillation detectors, which serve as the neutron analyzer, and 12 large-volume plastic-scintillation detectors, which detect neutrons scattered *up* or *down* by the analyzer detectors. Figures 5a and 5b show the side and plan views of this neutron polarimeter. Each layer of the front detector consists of two pieces of scintillator, each 25.4-cm high, by 50.8-cm long, by 10.16-cm thick, with one on top of the other. In each of the top and bottom rear detectors, there are two layers with each layer having three detectors set side by side horizontally with their long axis parallel to the incident neutron flux. Each detector has dimensions of 101.6-cm long by 50.8-cm wide by 10.16-cm high. The performance of another neutron polarimeter, configured with the same detectors and used by this group, proved to be successful in experiment E85-05 to measure G_E^n at Bates [Ed94]. Figure 6 shows the time-of-flight spectrum of an electron-neutron coincidence peak above a flat background obtained in the Bates experiment.

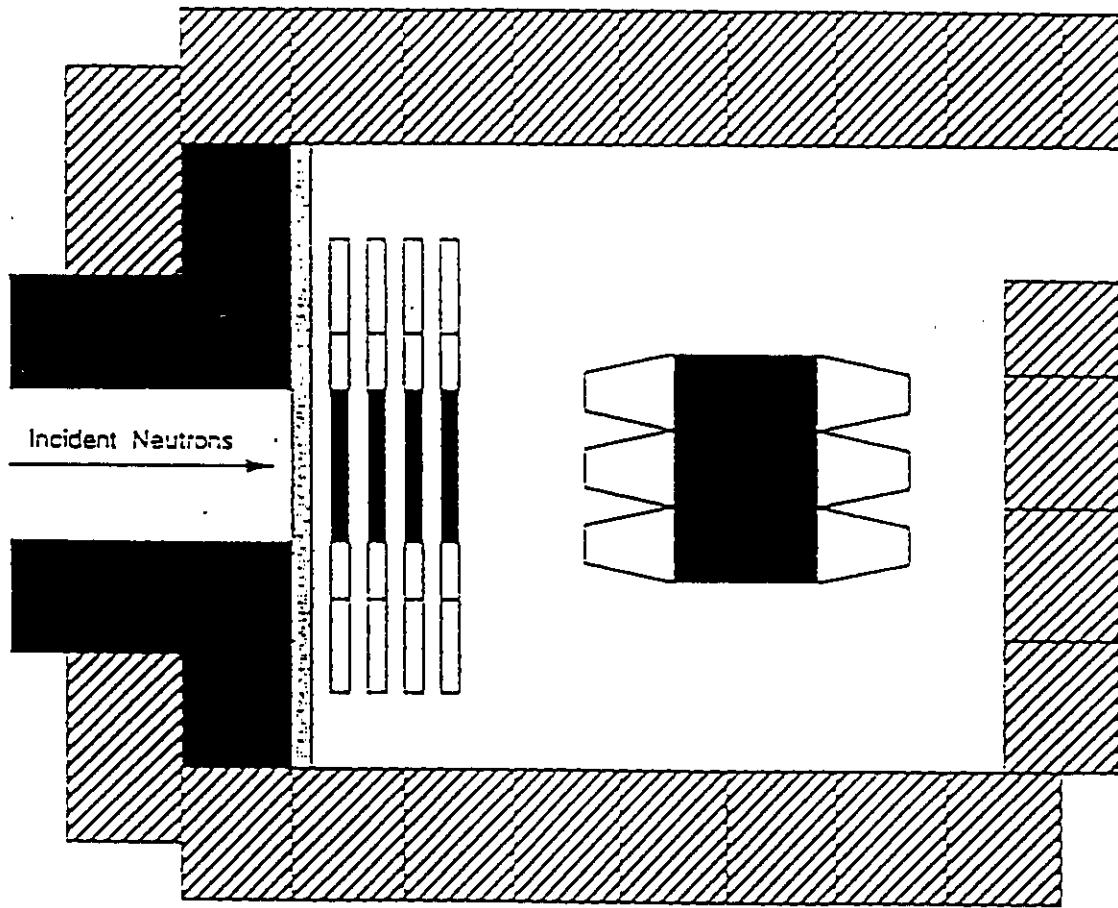
Neutron Polarimeter & Shielding



Side View

FIG. 5a: Side view of the neutron polarimeter.

Neutron Polarimeter & Shielding



Plan View

FIG. 5b: Plan view of the neutron polarimeter.

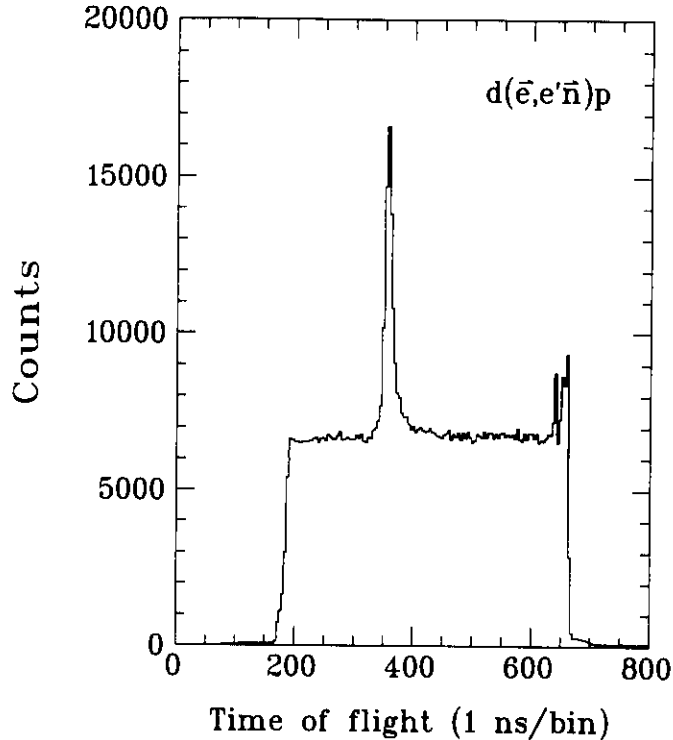


FIG. 6: Neutron time-of-flight spectrum from Bates experiment E85-05.

3.3 Steel Collimator and Shielding

In Fig. 5, the black blocks in front of the neutron polarimeter show the steel collimator (0.94-m thick), and the shadowed blocks show the concrete shielding walls. The rear wall and the two side walls are normal density ($\rho = 2.5 \text{ g cm}^{-3}$) concrete, 2.44-m thick. The roof of the enclosure is covered with normal-density concrete roof beams, 1.07-m thick. The wall in front of the neutron polarimeter consists of lead, 10.16-cm thick, poured into steel containers with 3.2-cm walls. The transmission of neutrons through this front shielding wall is about 0.38. Because this front shielding contains about 22 radiation lengths, the reduction in energy of a high-energy photon incident on this front shielding is expected to be so large as to be below the detection threshold. Because of the amount of shielding required, the

neutron polarimeter must be located at an angle of greater than 45° with respect to the beam line.

4 Design of the Experiment

4.1 Kinematics

We will perform the measurements at $Q^2 = 0.30 \text{ (GeV/c)}^2$. The kinematics are shown in Fig. 7 and listed in Table 1. The center-of-mass angle θ_{nq}^{cm} between the ejectile neutron and the three-momentum transfer \vec{q} (See Fig. 1) is chosen to be 38° . This is the widest angle possible because of the neutron polarimeter shielding. These kinematics are at quasielastic scattering and approximately “perpendicular” kinematics (where \vec{P}_r and \vec{P}' are approximately perpendicular). With a measurement on either side of \vec{q} , we can extract the response functions $R_{TT'}^t$ and $R_{LT'}^t$. In the future, it may be interesting to extend these measurements to non-quasielastic conditions, where the struck nucleon (the neutron) is excited into the “dip” or “ Δ ” regions.

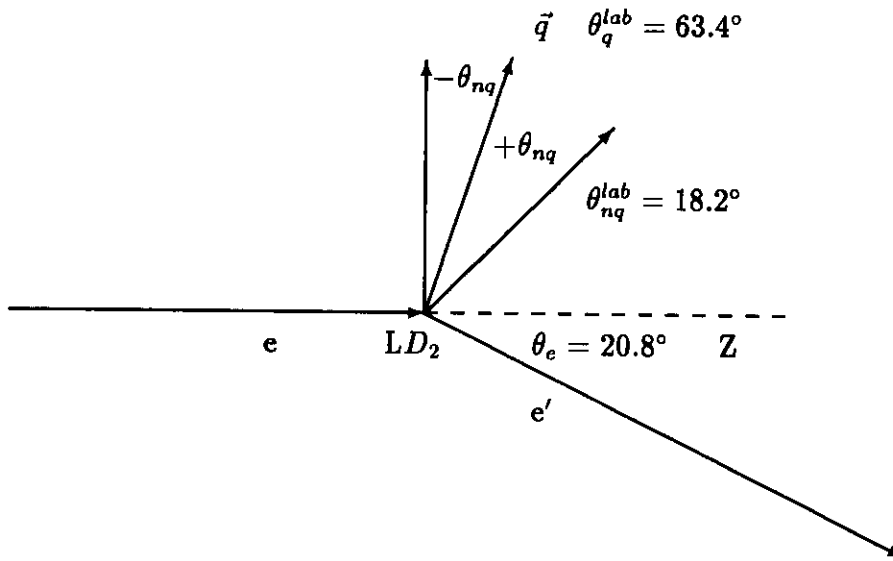


FIG. 7: Kinematic diagram for $Q^2 = 0.30 \text{ (GeV/c)}^2$.

Kin	E GeV	Q^2 (GeV/c) ²	\vec{q} MeV/c	ω MeV	E' GeV	p_r MeV/c	θ_{nq}^{cm} deg	T_n MeV	θ_e deg	θ_n deg
K^0	1.6	0.30	572.0	159.7	1.44	178.8	+38	142.3	20.8	-45.2
K^π	1.6	0.30	572.0	159.7	1.44	178.8	-38	142.3	20.8	-81.6

Table 1: Kinematics.

4.2 Conditions of Neutron Polarimeter and HMS

The analyzing power of the neutron polarimeter A_v is about 0.42, its detection efficiency ϵ is about 0.24%, and the flight path of the neutrons from the target the analyzers is 5.0 m. In this experiment, with nonzero recoil proton momentum, we use the full angular coverage of the HMS and the neutron polarimeter. The solid angle of HMS is about 5.62 msr, the solid angle of the neutron polarimeter is 20.7 msr. The neutron energy resolution is about 3.1 MeV (1.9%). The above experimental conditions are listed with others in Appendix A.

4.3 Beam and Targets

We plan to use the *low-intensity*, highly polarized electron beam ($P_b = 0.8$). We request beam currents of 0.67 and 5.0 μA for the two angles θ_{nq}^{cm} ; the low current at the one angle is required to reduce accidental background to an acceptable level. The liquid deuterium target is 15-cm thick ($\rho x = 2.55 \text{ g cm}^{-2}$). The luminosity L corresponding to the requested beam current of 5.0 μA and the 15-cm target thickness is $4.8 \times 10^{37} \text{ cm}^{-2} \text{ s}^{-1}$.

4.4 Counting Rate and Backgrounds

The counting rates and the backgrounds were calculated for the experimental conditions described in Appendix A. The calculated results and the cross sections used in the calculation are listed in Table 2.

Kin	$\frac{d^3\sigma}{dp_e d\Omega_e d\Omega_n}$ nb/(sr ² MeV/c)	$\frac{d^2\sigma}{d\Omega_e dp_e}$ nb/(srMeV)	$\frac{d\sigma}{d\Omega_n}$ μ b/sr	I μ A	L $10^{37} \text{ cm}^{-2} \text{ s}^{-1}$	R s^{-1}	A s^{-1}	R/A
K^0	0.25	12.6	2.0	0.67	0.64	0.018	0.018	1.0
K^π	0.47	12.6	0.50	5.0	4.8	0.26	0.26	1.0

Table 2: Cross sections and counting rates.

4.4.1 Counting Rate

Counting rates were calculated with the triple-differential cross sections averaged over the acceptances. The averaged triple-differential coincidence cross sections were calculated with the Monte Carlo code *MCEEP* of Ulmer [U191a]. The calculation of the counting rate for the K^0 kinematics condition is given in Appendix B.

4.4.2 Accidental Background

The accidental rate A was estimated by scaling the rate observed in Bates experiment E85-05 to the expected CEBAF conditions (luminosity, duty factor, fiducial cuts, single-arm cross sections *etc.*). The calculation of the accidental rate for the K^0 kinematics using this scaling method is also given in Appendix B. The neutron single-arm differential cross section was estimated with the electroproduction code *EPC* of Lightbody and O'Connell [Li88]; the electron single-arm differential cross section was obtained from the *MONQEE* code of Dytman, using the formulation of Moniz [Mo69].

4.4.3 Background from Inelastic Processes

The background from neutrons associated with inclusive inelastic processes $ed \rightarrow enX$ was estimated using the *CELEG* code by Joyce [Jo89] with the assumption that the cross section for the inclusive inelastic process is equal to that of the

quasifree elastic process. (Excitation-energy spectra reveal that these two cross sections are comparable [Bu68].) This estimation indicates that the background related to the inelastic processes is negligible at the planned beam energy of 1.6 GeV.

4.5 Statistics and Uncertainties

The absolute uncertainty in the transverse polarization observables is estimated by

$$\Delta p_t = \frac{(1 + K/r)}{A_y \sqrt{N}}, \quad (16)$$

where r is the signal-to-background ratio, N is the total number of neutron counts in the measurement, and K is a background correlation factor, which is estimated to be 0.7 using the data from Bates experiment E85-05 [Ed93a]. Based on the calculated event rates in Table 2 and the desired measurement uncertainties, we obtained the required number of counts N from Eq.(16) and the beam time from $T = N/R$. The results of these calculations and the estimated measurement uncertainties are summarized in Table 3. Shown in Fig. 2 with error bars are the measurement uncertainties in p_t and A_t at $Q^2 = 0.30$ (GeV/c)². The differences between the PWBA and PWBA + FIS calculations for A_t^+ at $\theta_{cm}^{nq} = 30^\circ$ is about three standard deviations of the measurements.

Kin	Time, T hrs	Counts, N 10^3	Δp_t	$\Delta A_t^\pm = \frac{1}{h\sqrt{2}} \Delta p_t$
K^0	224	14	0.034	0.030
K^π	16	14	0.034	0.030
Total	240			

Table 3: Uncertainties.

5 Beam Time Request

Because it will require at least a few days to move the neutron polarimeter, we request that the two angles be performed in two separate runs with at least one week in between. The first run would be at the angle with the higher counting rate and would include the majority of the set-up, testing, and calibrations; the second run would require shorter time for set-up and testing and then nine days for data acquisition. We request a total of 20 days of beam time, which includes three days for tuning and checkout, 10 days for data acquisition with an LD₂ target, and six days for tests (*viz.*, shadow shield, LH₂, and empty cell). The distribution of the beam time is listed in Table 4.

Activity	Time (Run 1) Days	Time (Run 2) Days	Total Days
Tuning and checkout of HMS	1	0.5	1.5
Checkout of NPOL and establish $e-n$ coincidence	1	0.5	1.5
Data acquisition with LD ₂ target	1	9	10
Test with LH ₂ and empty target	1	1	2
Test with shadow shield	0.5	1	1.5
Beam polarization measurements	1	1	2
Miscellaneous (overhead & contingency)	0.5	1	1.5
Total	6	14	20

Table 4: Distribution of beam time.

References

- [Ar81] R. G. Arnold, C. E. Carlson and F. Gross, *Phys. Rev. C* **23**, 363 (1981).
- [Ar91] H. Arenhövel and M. Sauzone, *Few Body Systems Supplementum* **3** (1991).
- [Ar94] H. Arenhövel, private communication (1994).
- [Au85] S. Auffret *et al.*, *Phys. Rev. Lett.* **54**, 649 (1985).
- [Bu68] W. Bartel *et al.*, *Phys. Lett.* **28B**, 287 (1968).
- [Dm89] V. Dmitrasinovic and Franz Gross, *Phys. Rev. C* **40**, 2479 (1989).
- [Ed94] T. Eden *et al.*, submitted to *Phys. Lett. B* (March 1994).
- [Fa78] W. Fabian and H. Arenhövel, *Nucl. Phys.* **A314**, 253 (1978).
- [Fi89] S. J. M. Finn, P. E Ulmer, and the Hall A collaboration, CEBAF proposal E89-028 (1989).
- [Fr84] S. Frullani and J. Mougey, *Adv. in Nucl. Phys.* **14**, 1 (1984).
- [Hu94] E Hummel and J. A. Tjon, *Phys. Rev. C* **14**, 21 (1984).
- [Jo89] D. Joyce, CLAS (CEBAF) Note 89-004 (1989).
- [Li88] J. W. Lightbody and J. S. O'Connell, *Computers in Physics* (1988).
- [Ma94] R. Madey, *et al.*, CEBAF proposal E93-038 (1994).
- [Ma94a] R. Madey, A. Lai, and T. Eden, *Bull. Am. Phys. Soc.* **39**, 1055 (1994).
- [Mo69] E. Moniz, *Phys. Rev.* **184**, 1154 (1969).
- [Mo76] J. Mougey *et al.*, *Nucl. Phys. A* **262**, 461 (1976).
- [Pi87] A. Picklesimer and J. W. Van Orden, *Phys. Rev. C* **35**, 266 (1987).

- [Pi89] A. Picklesimer and J. W. Van Orden, *Phys. Rev. C* **40**, 290 (1989).
- [Si79] G. G. Simon *et al.*, *Nucl. Phys. A* **324**, 277 (1979).
- [Ul91] P. Ulmer *et al.*, Bates Proposal “Extension of E88-21” (1991).
- [Ul91a] P. Ulmer, CEBAF Technical Note 91-101 (1991).
- [Wi93] T. Wilbois, G. Beek, and H. Arenhövel, *Few-Body System* **15**, 39 (1993).
- [Ed93a] T. Eden, Ph.D. Dissertation, Kent State University (1993).

Appendix A

Experimental Conditions [$Q^2 = 0.30 \text{ (GeV/c)}^2$, $\theta_{nq}^{cm} = 38^\circ$]

1. Electron Beam

Energy, E (GeV)	1.6
Polarization, P_L	0.80
Current, I (μA)	0.67–5.0
Incident electron flux, $F(10^{14} \text{ e/s})$	0.93
Duty factor	1.0

2. Liquid Deuterium Target Cell

LD ₂ thickness, ρx (g/cm^2) [= (0.168 g/cm^3) (15.0 cm)]	2.55
Power dissipation, P (Watts)	35.1

3. Luminosity $F \rho_n x = L$ ($\text{cm}^{-2} \text{ s}^{-1}$)

Luminosity for deuterium, L_2 ($\text{cm}^{-2} \text{ s}^{-1}$)	$(0.64 - 4.8) \times 10^{37}$
---	-------------------------------

4. Neutron Polarimeter

Height of analyzer detectors, h (m)	0.508
Width of analyzer detectors, w (m)	1.016
Mean flight path, x (m)	5.00
Horizontal angular acceptance, $\Delta\theta_n$	$\pm 5.92^\circ$
Vertical angular acceptance, $\Delta\phi_n$	$\pm 2.90^\circ$
Solid angle, $\Delta\Omega_n$ (msr)	20.7
Efficiency, ϵ (%)	0.24
Average analyzing power, \overline{A}_y	0.42
Neutron transmission through Pb-Fe shielding, t	0.38
Neutron energy resolution T (MeV)	3.1
Relative energy resolution $\Delta T/T$ (%)	1.9

5. Electron Spectrometer

Horizontal angular acceptance, $\Delta\theta_e$	$\pm 62.0 \text{ mr} = \pm 3.50^\circ$
Vertical angular acceptance, $\Delta\phi_e$	$\pm 22.5 \text{ mr} = \pm 1.29^\circ$

Solid angle, $\Delta\Omega_e$ (msr)	5.62
Momentum acceptance, $\Delta p_e/p_e$ (%)	± 5.0
Momentum bite, $\Delta p_e = \pm 0.050 p_e$ (MeV/c)	± 72
Efficiency for a “good” electron, ϵ_{wc}	~ 0.97
Live-time fraction in wire chambers, l_{wc}	~ 0.95
Radiative correction factor, ϵ_{rad}	0.83

6. Data Acquisition System

Live-time fraction, l	0.95
-------------------------	------

Appendix B

Counting Rate and Background at Kinematic K^0

I. Counting Rate R

The electron-neutron coincidence counting rate R can be estimated as follows:

$$\begin{aligned}
 R &= L \langle \sigma_3(p_e, \theta_e, \theta_n) \rangle (2\Delta p_e) \Delta \Omega_e \Delta \Omega_n \epsilon_n \epsilon_{wc} l_{wc} \epsilon_{rad} l t \\
 &= 0.64 \times 10^{37} \times 0.25 \times 10^{-33} \times (2 \times 72) \times 5.62 \\
 &\quad \times 20.7 \times 0.24\% \times 0.95 \times 0.83 \times 0.95 \times 0.38 \text{ s}^{-1} \\
 &= 0.018 \text{ s}^{-1}
 \end{aligned} \tag{1}$$

II. Accidental Rate A

To estimate the accidental coincidence counting rates A^C expected at CEBAF, we scale our results from the accidental rates $A^B = 0.035 \text{ s}^{-1}$ observed for Bates E85-05:

$$\begin{aligned}
 A^C &= \frac{f^B \tau^C N_e^C N_n^C f^B}{f^C \tau^B N_e^B N_n^B f^C} \\
 &= \frac{f^B \tau^C (L^C)^2 [d^2 \sigma^C / (d\Omega_e dp_e)] \Delta \Omega_e^C \Delta p_e^C (d\sigma^C / d\Omega_n) \Delta \Omega_n^C \epsilon^C}{f^C \tau^B (L^B)^2 [d^2 \sigma^B / (d\Omega_e dp_e)] \Delta \Omega_e^B \Delta p_e^B (d\sigma^B / d\Omega_n) \Delta \Omega_n^B \epsilon^B} A^B \\
 &= \frac{0.008 \ 0.7 \ (0.64)^2 \times 12.6 \times 5.62 \times 72 \times 2.0 \times 20.7 \ 0.24}{1.0 \ 2.0 \ (0.26)^2 \times 5.4 \times 5.62 \times 32.4 \times 0.72 \times 9.68 \ 0.21} \times 0.035 \text{ s}^{-1} \\
 &= 0.018 \text{ s}^{-1}.
 \end{aligned} \tag{2}$$

In Eq.(2), the symbols with superscript of B and C represent quantities at Bates and CEBAF, respectively. The values of the quantities at Bates can be found in CEBAF proposal E93-038 [Ma94].